# RESEARCH STUDIES ON OBTAINING METASTABLE INTERMETALLIC STRUCTURES IN 6xxx/BORIDES COMPOSITES

Mihai BUȚU[1], Petru MOLDOVAN[2], Lucian ROȘU [3]*, Constantin STĂNCEL[4], Cătălin OGICA[5], Larisa BUȚU[6], Marilena MARINESCU[7]

*The paper presents data on the metastable structures obtained by solidifying the 6xxx/$MeB_2$ composites, elaborated by aluminothermic reactions between salts ($K_2TiF_6$, $K_2ZrF_6$, $KBF_4$), pre-alloys (AlV10) and AA6060 or AA6063, in the presence of cryolite ($Na_3AlF_6$). Through MO, ME (SEM/TEM) and X-ray diffraction the obtained intermetallic structures were highlighted with some properties characteristic of hexagonal, tetragonal and rhombic crystallographic systems.*

**Keywords:** $TiB_2$, $ZrB_2$, $VB_2$, intermetallic compounds, MMCs, crystallographic system

## 1. Introduction

Aluminium matrix composites and reinforcement particles obtained by aluminothermic reactions are increasingly sought for their properties and for their ease of elaboration. The main Al alloys used as the matrix are those in the 6xxx series, with a low content of alloying / microalloying elements. (for eg. AA6060 and AA6063). These alloys contain low concentrations of silicon (~ 0.45% Si in AA6060 and ~ 0.7% Si in AA6063), magnesium (~ 0.5% Mg in AA6060 and ~ 0.4% Mg in AA6063) and iron (~ 0.25% Fe in AA6060 and ~ 0.4% Fe in AA6063). The paper presents the possible crystalline structures obtained by solidification in the ternary and quaternary systems containing the Al, Mg, Si and

[1] Faculty of Materials Science and Engineering, University POLITEHNICA of Bucharest, Romania, e-mail: mihaibutu@yahoo.com
[2] Faculty of Materials Science and Engineering, University POLITEHNICA of Bucharest, Romania, e-mail: cavnic2010@yahoo.com
[3]* Faculty of Materials Science and Engineering, University POLITEHNICA of Bucharest, Romania, e-mail: rosu.lucian@mail.
[4] Faculty of Materials Science and Engineering, University POLITEHNICA of Bucharest, Romania, e-mail: stancel.constantin@yahoo.com
[5] Faculty of Materials Science and Engineering, University POLITEHNICA of Bucharest, Romania, e-mail: catalin66@gmail.com
[6] Faculty of Industrial and Robotic Engineering, University POLITEHNICA of Bucharest, Romania, e-mail: l_butu@yahoo.com
[7] Faculty of Industrial and Robotic Engineering, University POLITEHNICA of Bucharest, Romania, e-mail: m_marinescuro@yahoo.com

Fe, elements with the transformations that can occur and the resulting compounds from solidification under equilibrium conditions.

**Al-Mg-Si** alloys have started to be used more and more in the automotive and aerospace industries, especially for critical structures, due to the fact that they can be easily cast, they are corrosion resistant and last but not least, for their good and very good mechanical properties, especially after heat treatment. In these alloys, Mg is intentionally introduced to be able to induce artificial ageing by precipitating the metastable $Mg_2Si$ phase or in order to form Guinier-Preston areas. [1 ÷ 9]. The Guinier-Preston zones are small-scale metallurgical phenomena that involve precipitation in the early stages of the metastable $Mg_2Si$ phase. GP areas are associated with the ageing phenomenon, where reactions at room temperature continue to occur in material over time, leading to a change in physical properties. This happens especially in the 6xxx and 7xxx aluminium alloy series. From a physical point of view, the GP areas are extremely fine (dimensions of 3-10 nm) areas with high concentrations of $Mg_2Si$ [2].

In the literature, the temperature of the pseudo-binary eutectic presents several values: 595°C [3], [5], [7], 593°C [8], 590 [2], 597°C [4], [9]. Using the thermodynamic parameters of the model reported by [3], the calculated temperature is 594°C. In the Al-Mg-Si phase diagram [11], in the corner with high aluminium concentration, it is observed that Al can be in equilibrium with $Mg_2Si$, $Al_8Mg_5$ or (Si). The quasi-binary cross-section between (Al) and $Mg_2Si$ corresponds to the concentration ratio of Mg:Si = 1.73. This cross-section divides the phase diagram into two simple eutectic diagrams: Al-Mg-$Mg_2Si$ and Al-Si-$Mg_2Si$. The invariable phase transformations that take place in this system are: L → (Al) + $Mg_2Si$ (quasi-binary cross-section at 595°C; L → (Al) + (Si) + $Mg_2Si$ at 555°C; L → (Al) + $Mg_2Si$ + $Al_8Mg_5$ at 449°C.

The $Mg_2Si$ compound (63.2% Mg, 36.8% Si) has a cubic structure (Fm3m, 12 atoms/cell unit) with the lattice parameter of a = 0,635 ÷ 0,640 nm, has a melting temperature of 1087°C, density $\rho$ = 1.88 g/cm$^3$, Vickers hardness HV = 4.5 GPa [10]. The micro-hardness of the $Mg_2Si$ compound at room temperature is 5.36 GPa, while the micro-hardness after one hour at 300°C is 1.77 GPa – this being an indicator of its low thermal stability.

The **Al-Fe-Si** system is used for the analysis of 1xxx alloys, of pure commercial aluminium with minor impurities of Fe and Si and of the Al-Si binary alloys (which, as a rule, contain certain amounts of Fe impurities). Detailed studies of the Al-Fe-Si phase diagram were performed in ref. [11], where detailed files of the liquidus, solidus and solvus isotherms can be found, as well as intermediate phase transformations. It is generally accepted today that (Al) can be in equilibrium with (Si), $Al_3Fe$, $Al_8Fe_2Si$ and $Al_5FeSi$, which can participate in different invariable phase transformations: L → (Al) + $Al_5FeSi$ + (Si) at 576°C; L + $Al_8Fe_2Si$ → (Al) + $Al_5FeSi$ at 629°C; L + $Al_3Fe$ → (Al) + α$Al_8Fe_2Si$ at 611°C

The solubility of iron in silicon is very small, even negligible [11]. $Al_8Fe_2Si$ compound (31,6% Fe, 7,8% Si) it is also noted as $Al_{12}Fe_3Si_2$ (30,7% Fe, 10,2% Si), $Al_{7,4}Fe_2Si$, $\alpha$(AlFeSi) or $c$(AlFeSi). The compound appears at the concentration of 30 ÷ 33% Fe, 6 ÷ 12% Si and has a hexagonal structure (space group P63/mmc) with the lattice parameters of $a$ = 1.23 ÷ 1.24 nm, $c$ = 2.62 ÷ 2.63 nm. The density of this phase is 3.58 g/cm$^3$ [11].

$Al_5FeSi$ phase (25,6% Fe, 12,8% Si) is also noted as $Al_9Fe_2Si_2$, $\beta$(AlFeSi) and $m$(AlFeSi); it exists at the concentration of 25 ÷ 30% Fe, 12 ÷ 15% Si. This phase has a monoclinic structure with the following parameters a = $b$ = 0.612 nm, $c$ = 4.148 ÷ 4.150 nm, $\beta$ = 91° [11]. Its density is 3.3 ÷ 3.6 g/cm$^3$, Vickers hardness HV = 5.8 GPa [11] [12]. $\beta$(AlFeSi) micro-hardness at 20°C is 11.47 GPa, while the micro-hardness after one hour at 300°C is 7.85 GPa (meaning that this is a phase with exceptional thermal stability) [11].

Other ternary compounds are: $Al_4FeSi_2$ (25.4% Fe, 25.5% Si), noted as $Al_3FeSi_3$, $\delta$(AlFeSi) or $t$(AlFeSi), which has a range of homogeneity that is narrower than that of $\alpha$(AlFeSi) or $\beta$(AlFeSi) – this phase has a tetragonal structure of type $PdGa_5$ with the following parameters: $a$ = 0.607 ÷ 0.63 nm, $c$ = 0.941 ÷ 0.953 nm, with density ρ = 3.3 ÷ 3.36 g/cm$^3$ [10] [12], micro-hardness at 20°C equal to 10.97 GPa and micro-hardness after one hour at 300°C 5.18 GPa [10]; $Al_3FeSi$ (33.9% Fe, 16.9% Si), sometimes noted as γ(AlFeSi), which has a monoclinic structure with the lattice parameters a = 1.78 nm, b = 1.025 nm, c = 0.890 nm and $\beta$ = 130° [11].

Due to this complexity, real industrial alloys may contain coexisting phases, such as $Al_3Fe$, $Al_6Fe$, $\alpha$(AlFeSi), $\beta$(AlFeSi) and $\delta$(AlFeSi). The identification of these phases is often a very difficult problem because the same phase can have very different morphologies as a function of their origin: primary crystals (constituent particles) or the products of peritectic and eutectic phase reactions.

**Al-Fe-Mg system.** The analysis of this phase diagram offers the possibility to track the role and influence of the additions and impurities of iron on the phase composition of Al-Mg foundry alloys containing small quantities of silicon, manganese and other possible elements. There are no ternary compounds in the Al-Fe-Mg phase diagram [11] [12]. (Al) can be in equilibrium with the binary phases $Al_3Fe$ and $Al_8Mg_5$. There is only one invariable eutectic phase transformation in the high-concentration aluminium corner of this system: L → (Al) + $Al_3Fe$ + $Al_8Mg_5$ at 451°C or at 445°C. The solubility of Mg in $Al_3Fe$ and Fe in $Al_8Mg_5$ is negligible. The solubility of iron in aluminium decreases with the addition of magnesium. Instead, Fe substantially decreases the solubility of magnesium in aluminium, which has 14% Mg at the ternary eutectic temperature [12].

***The Al-Fe-Mg-Si system.*** This system is important for many foundry industrial alloys, especially Al-Si and Al-Mg. This is, first of all, related to the existence of the quaternary compound, which makes it impossible to analyse the ternary phase diagrams in order to determine the composition of the alloy phase. The quaternary compound, often designated as the π phase, has a narrow homogeneity range around the composition corresponding to the $Al_8FeMg_3Si_6$ (10.9% Fe, 14.1% Mg, 32.9% Si) chemical formula. In addition to this quaternary phase, (Al) can be in equilibrium with $Al_3Fe$, $Al_8Mg_5$, $Mg_2Si$, $Al_8Fe_2Si$, $Al_5FeSi$ and (Si) [12]. Fig. 1 shows the projection of the liquidus surface (a) and the distribution of the phase fields in solid-state (b) for the alloys of the Al-Fe-Mg-Si system. The invariable phase transformations in this system are shown in [12]. There is an (Al)-$Mg_2Si$ quasi-binary cross-section in this system, which is why an (Al)-$Mg_2Si$-$Al_3Fe$ quasi-ternary cross-section can be defined, which divides the Al-Fe-Mg-Si phase diagram in two parts (Figure 1).

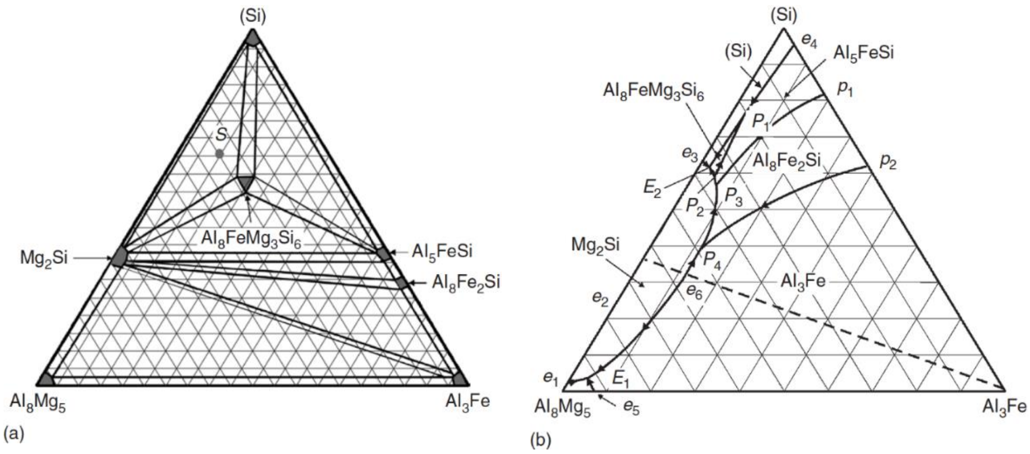


Figure 1. Al-Fe-Mg-Si quaternary phase diagram: (a) polythermal diagram and (b) the distribution of the phase fields in the solid-state in the high concentration aluminium corner [11]

$Al_8FeMg_3Si_6$ phase (noted as $\pi$ or $h$(AlFeMgSi)) crystallizes in hexagonal system (space group P62m, 18 atoms/cell unit) with lattice parameters a = 0.663 nm, c = 0.794 nm. The density of this phase is $\rho = 2.82\ g/cm^3$ [12]. Micro-hardness at room temperature si equal to 5.85 GPa, while the micro-hardness at 300°C (one hour holding) is 3.76 GPa [13], which is why the phase is considered to have good thermal stability. Invariable phase transformations in the Al-Fe-Mg-Si system, in the corner with high concentration of aluminium are the following: L → (Al) +$Al_3Fe$ + $Mg_2Si$ at > 587°C; L + $Al_3Fe$ → (Al) + $Mg_2Si$ + $Al_8Fe_2Si$ at 586°C; L + $Al_8Fe_2Si$ → (Al) + $Mg_2Si$ + $Al_5FeSi$ at 576°C; L + $Al_5FeSi$ → (Al) + $Mg_2Si$ + $Al_8FeMg_3Si_6$ at 568°C; L + $Al_5FeSi$ → (Al) + (Si) + $Al_8FeMg_3Si_6$ at 567°C; L → (Al) + (Si) + $Mg_2Si$+ $Al_8FeMg_3Si_6$ at 554°C and L → (Al) + $Al_3Fe$ + $Al_8Mg_5$ + $Mg_2Si$ at 448°C.

It is clear that the solidification domain of the quaternary phase is relatively small and is located to some extent outside the homogeneity domain of this compound ($Al_8FeMg_3Si_6$) in the solid phase. It should also be noted that the $Mg_2Si$ phase it is in balance with all other phases and can be present in most alloys in solid-state. Under solidification conditions outside the equilibrium, most of the peritectic reactions will not be completed, and the alloys will contain a larger number of phases than could be predicted according to the corresponding equilibrium phase diagram.

## 2. Elaboration of AA6060, AA6063 / $MeB_2$ composites by aluminothermic reactions

The proposed procedure for the experimental part is the in-situ aluminothermic reaction between the molten aluminium alloys AA6060 and AA6063, which act as the matrix, potassium hexafluorotitanate ($K_2TiF_6$) which is a titanium supplier, potassium tetrafluoroborate ($KBF_4$) which is the boron supplier for the formation of $TiB_2$, between potassium hexafluorozirconate ($K_2ZrF_6$) and potassium tetrafluoroborate ($KBF_4$), for the formation of $ZrB_2$, between potassium tetrafluoroborate ($KBF_4$) and AlV10 pre-alloy, for obtaining vanadium diboride ($VB_2$), all in the presence of cryolite ($Na_3AlF_6$) to prevent the formation of aluminium oxide barriers ($Al_2O_3$).

*Table 1*

**The standardized and nominal composition of 6xxx series alloys, wt.%**

| | Component, Wt.% | | | | | | | | | |
|---|---|---|---|---|---|---|---|---|---|---|
| Alloy | Al | Mg | Si | Cr | Mn | Ti | Cu | Fe | Zn | Other |
| AA6063 | 97.5 | 0.45 – 0.9 | 0.2 – 0.6 | 0.1 Max | 0.1 Max | 0.1 Max | 0.1 Max | 0.35 Max | 0.1 Max | 0.15 Max |
| Nominal | 98.29 | 0.72 | 0.49 | 0.06 | 0.02 | 0.04 | 0.02 | 0.33 | 0.03 | |

| | | | | | | | | | | |
|---|---|---|---|---|---|---|---|---|---|---|
| AA6060 | 97.8 | 0.35 – 0.60 | 0.30 – 0.60 | 0.05 Max | 0.1 Max | 0.1 Max | 0.1 Max | 0.10 – 0.30 | 0.15 Max | 0.15 Max |
| Nominal | 98.852 | 0.429 | 0.439 | 0.003 | 0.014 | 0.013 | 0.012 | 0.221 | 0.017 | |

The main intermetallic compound present in solidification in the studied alloys (AA6060/AA6063) is $Mg_2Si$ with the characteristics presented in Fig. 2.

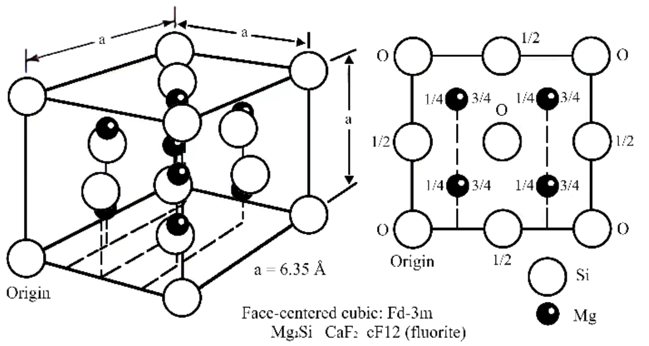


| $Mg_2Si$ | |
|---|---|
| Crystal system: | Cubic |
| Space group: | Fd$\bar{3}$m |
| Space group number: | 227 |
| a = b = c (nm): | 0.63515 |
| $\alpha = \beta = \gamma$ (°): | 90 |
| Volume of the cell ($10^6$ $pm^3$) | 256.23 |
| Z: | 8.00 |

Fig. 2. Atom positions, prototype, structure symbols, space-group notations, and lattice parameters for the $Mg_2Si$ metallic crystal *[14]*

Following the aluminothermic reactions between the AA6060, AA6063 alloys and the salts mentioned above, the following intermetallic compounds can be obtained: $TiB_2$ (reaction 1), $TiAl_3$ (reaction 2), $TiAl_2$ (reaction 3), $ZrB_2$ (reaction 4), $ZrAl_3$ (reaction 5), $VB_2$ (reaction 6).

$$3K_2TiF_6 + 6KBF_4 + 10Al = 4K_3AlF_6 + 6AlF_3 + 3\mathbf{TiB_2} \quad (1)$$
$$3K_2TiF_6 + 13Al = 3\mathbf{Al_3Ti} + 6KF + 4AlF_3 \quad (2)$$
$$3K_2TiF_6 + 10Al = 3\mathbf{Al_2Ti} + 6KF + 4AlF_3 \quad (3)$$
$$3K_2ZrF_6 + 6KBF_4 + 10Al = 4K_3AlF_6 + 6AlF_3 + 3\mathbf{ZrB_2} \quad (4)$$
$$6KBF_4 + 6K_2ZrF_6 + 23Al = 3\mathbf{Al_3Zr} + 3ZrB_2 + 6K_3AlF_6 + 8AlF_3 \quad (5)$$
$$6KBF_4 + 3V + 6Al = 3\mathbf{VB_2} + 2K_3AlF_6 + 4AlF_3 \quad (6)$$

These intermetallic structures have exceptional properties. The structural characteristics of the compounds that may result from the reactions (1) - (6) are presented in Table *Table* 2.

*Table 2*

**Physical properties of the borons studied [16]**

| IUPAC name | Theoretical chemical formula, [CASRN] | Crystal system, lattice parameters. Pearson symbol, space group, structure type, Z | Thermal conductivity ($k.Wm^{-1}K^{-1}$) | Specific heat capacity ($c_p$.J $kg^{-1}$ $K^{-1}$) | Coefficient of linear thermal expansion ($\alpha$, $10^{-6}$ $K^{-1}$) |
|---|---|---|---|---|---|
| Titanium diboride | $TiB_2$ [12045-63-5] | Hexagonal $a$ = 0,3028 nm $c$ = 0,3228 nm, | 64.4 | 637.33 | 7.6-8.6 |

| | | | | | |
|---|---|---|---|---|---|
| | 69.489 | *hP*3, *P*6/*mmm*, $AlB_2$ type (*Z* = 1) | | | |
| Zirconium diboride | $ZrB_2$ [12045-64-6] 112.846 | Hexagonal *a* = 0,3169 nm c = 0,3530 nm *hP*3, *P*6/*mmm*, $AlB_2$ type (*Z* = 1) | 57.9 | 392.54 | 5.5-8.3 |
| Vanadium diboride | $VB_2$ [12007-37-3] 72.564 | Hexagonal *a* = 0,2998 nm c = 0,3057 nm *hP*3, *P*6/*mmm*, $AlB_2$ type (*Z* = 1) | 42.3 | 647.43 | 7.6-8.3 |

In addition to the properties presented in Table 2, the diborides of the transition metal (Ti, Zr, V) also have other characteristics/properties:

• ***$TiB_2$.*** Gray crystals, superconducting at 1.26 K. High-temperature electrical conductor, used in the form of a cermet as a crucible material for handling molten metals such as Al, Zn, Cd, Bi, Sn, and Rb. It is strongly corroded by liquid metals such as Tl, Zr, V, Nb, Ta, Cr, Mn, Fe, Co, Ni, and Cu. Begins to be oxidized in the air above 1100–1400◦C. Corrosion-resistant in hot concentrated brines [16]. Maximum operating temperature 1000°C (reducing environment) and 800°C (oxidizing environment), has a density of 4.52 g/cm$^3$, melting temperature between 2980 ÷ 3225°C and 3370 HV Vickers hardness.

• ***$ZrB_2$.*** Gray metallic crystals, excellent thermal-shock resistance, greatest oxidation inertness of all refractory hard metals. Hot-pressed material is used in crucibles for handling molten metals such as Zn, Mg, Fe, Cu, Zn, Cd, Sn, Pb, Rb, Bi, Cr, brass, carbon steel, and cast iron, and also molten cryolite, yttria, zirconia, and alumina. It is readily corroded by liquid metals such as Si, Cr, Mn, Co, Ni, Nb, Mo, and Ta, and attacked by molten salts such as $Na_2O$, alkali carbonates, and NaOH. Severe oxidation in air occurs above 1100–1400°C. Stable above 2000°C under inert or reducing atmosphere [16], has a density of 6,085 g/cm$^3$, melting temperature between 3060 ÷ 3245°C and Vickers hardness with values between 1900 and 3400 HV.

• ***$VB_2$.*** Wear-resistant, semiconducting films [16], has a density of 5.070 g/cm$^3$, melting temperature between 2450 ÷ 2747°C and Vickers hardness with values between 1750 and 4234 HV determined on in-situ obtained particles from the AA6063/$VB_2$ composite, using the Leco M-400-G micro-hardness tester, with the average hardness of $HV_{med}$ = 2491.

The crystallographic data of the intermetallic compounds resulting from reactions (1) - (6) are presented in Table 3.

*Table 3*

**The crystallographic characteristics of the studied intermetallic compounds**

| | $TiB_2$ | $TiAl_3$ | $TiAl_2$ | $ZrB_2$ | $Al_3Zr$ | $VB_2$ |
|---|---|---|---|---|---|---|
| Crystal | Hexagonal | Tetragonal | Orthorhombic | Hexagonal | Tetragonal | Hexagonal |

| | | | | | | |
|---|---|---|---|---|---|---|
| system: | | | | | | |
| Space group: | P6/mmm | I4/mmm | Cmmm | P6/mmm | I4/mmm | P6/mmm |
| Space group number: | 191 | 139 | 65 | 191 | 139 | 191 |
| a (nm): | 0.30296 | 0.38537 | 1.20944 | 0.31670 | 0.40140 | 0.29976 |
| b (nm): | 0.30296 | 0.38537 | 0.39591 | 0.31670 | 0.40140 | 0.29976 |
| c (nm): | 0.32260 | 0.85839 | 0.40315 | 0.35300 | 1.73200 | 0.30562 |
| $\alpha$ (°): | 90 | 90 | 90 | 90 | 90 | 90 |
| $\beta$ (°): | 90 | 90 | 90 | 90 | 90 | 90 |
| $\gamma$ (°): | 120 | 90 | 90 | 120 | 90 | 120 |
| Volume of cell ($10^6$ $pm^3$) | 25.68 | 127.48 | 193.04 | 30.66 | 279.06 | 23.78 |
| Z: | 1.00 | 2.00 | 4.00 | 1.00 | 4.00 | 1.00 |

### 3. Characterization of the obtained intermetallic compounds

Depending on the quantities of salts used in order to obtain the AA6060, AA6063 / $MeB_2$ composites, where Me is Ti, Zr or V, on the working temperature and the solidification conditions, different intermetallic structures ($TiB_2$, $TiAl_3$, $TiAl_2$, $ZrB_2$, $ZrAl_3$ and $VB_2$) can be obtained as evidenced by optical microscopy (Olympus BX51M with Olympus UC30 camera and Olympus Stream Essentials software), electron microscopy (FEI Quanta Inspect F Microscope) and X-ray diffraction (D8 ADVANCE type BRUCKER-AXS / $ZrB_2$ and $VB_2$, Panalytical X'PERT PRO / $TiB_2$).

Fig. 3 shows the obtained $TiB_2$ particles. Through the analysis by optical microscopy, it can be observed that the particle sizes of $TiB_2$ do not exceed the size of 2μm. In order to highlight these particles, a sample of AA6060/$TiB_2$ composite was solubilized in concentrated hydrochloric acid, washed several times with distilled water and the resulting powder was dried in a drying stove and then analysed by TEM. (b). Fig. 4 shows the X-ray diffraction.

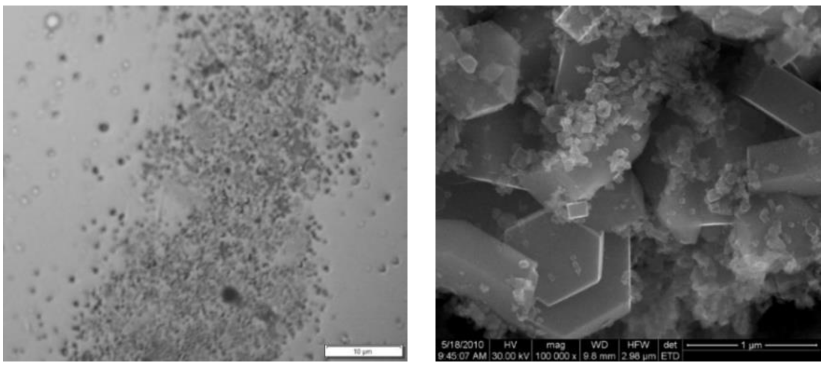

(a) (b)

Fig. 3. Optical microstructure (a) and TEM micrograph of the AA6060/$TiB_2$ composites

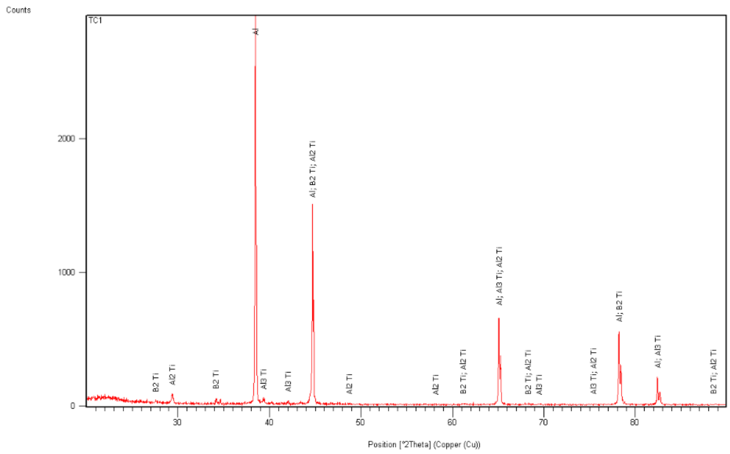


Fig. 4. Composite diffractogram AA6060/$TiB_2$, $TiAl_3$ and $TiAl_2$

The obtained $TiB_2$ compound crystallizes in the hexagonal system, space group P6/mmm, with lattice parameters a = 0.30325 nm and c = 0.32313 nm. The $TiAl_3$ compound crystallizes in the tetragonal system, space group I4/mmm, with lattice parameters a = 0.384 nm and c = 0.859 nm. The obtained $TiAl_2$ compound crystallizes in the rhombic system, space group Cmmm with lattice parameters a = 0.120944 nm, b = 0.3959 nm, c = 0.40315 nm, with the calculated density $\rho$ = 3.51 g/cm$^3$.

Fig. 5 shows the obtained $ZrB_2$ particles. By optical microscopy analysis, it is observed that the particle sizes of $ZrB_2$ have values up to 2 μm. In order to highlight these particles, a sample of AA6063/$ZrB_2$ composite was solubilized in concentrated hydrochloric acid, washed several times with distilled water and the resulting powder was dried in a drying stove and then analysed by TEM. (b). Fig. 6 shows the general diffraction of the AA6063 composites reinforced with $ZrB_2$ and $VB_2$ respectively and in Fig. 7 the peaks of the $ZrB_2$ and $Al_3Zr$ compounds are shown.

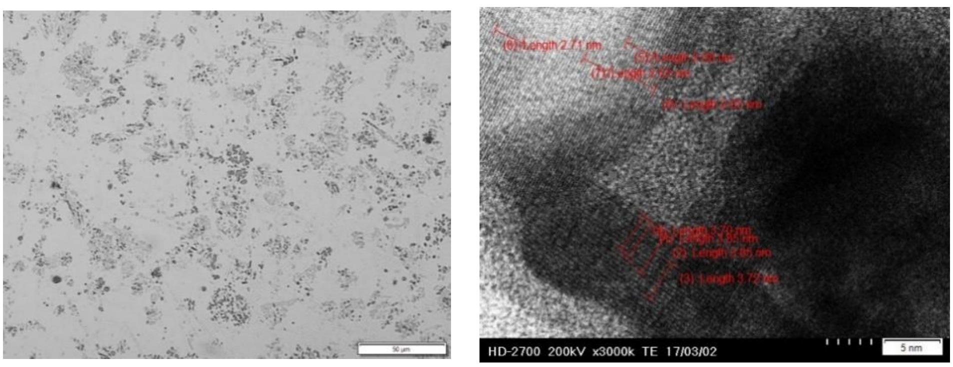


(a) (b)

Fig. 5. Optical microstructure (a) and TEM micrograph of the AA6063/$ZrB_2$ composites

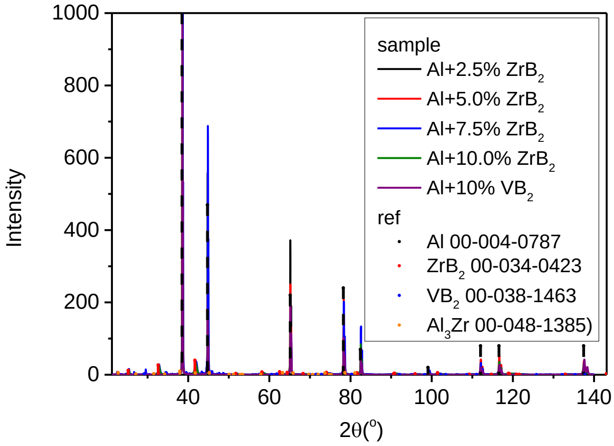


Fig. 6. X-ray diffraction of the AA6063/$ZrB_2$ and AA6063/$VB_2$ composites

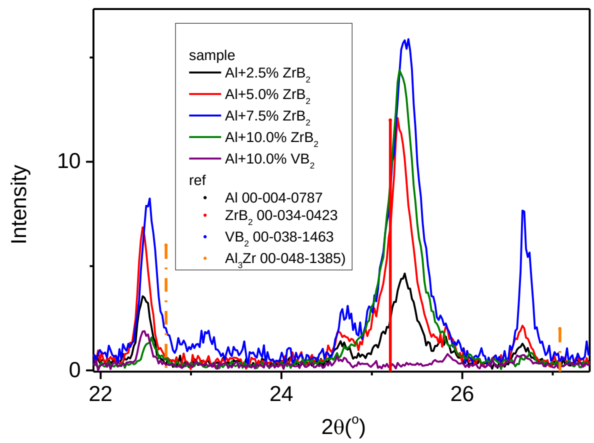


Fig. 7. X-ray diffraction of the AA6063/$ZrB_2$ and AA6063/$VB_2$ composites, with highlighted $ZrB_2$ and $Al_3Zr$ peaks

The obtained $ZrB_2$ compound crystallizes in hexagonal system, with structure type $AlB_2$, Pearson symbol hP3, space group P6/mmm with lattice parameters a = 0.3169 nm, c = 0.3530 nm and the calculated density ρ = 6.104 g/cm$^3$ (00-034-0423, D8 ADVANCE type BRUCKER-AXS). An in-depth analysis of the crystalline structure of the ZrB2 compound, using the .......... electron microscope, revealed, for two analysed areas, the following lattice parameter dimensions: $a_1$ = 0.262 ÷ 0.271 nm and $c_1$ = 0.370 ÷ 0.385 nm.

The obtained $Al_3Zr$ compound crystallizes in tetragonal system, with structure type $Al_3Zr$, Pearson symbol tI16, I4/mmm space group with lattice parameters a = 0.4009 nm, c = 1.7281 nm and the calculated density ρ = 4.117 g/cm$^3$.

Fig. 8 shows the obtained $VB_2$ particles. Analysing using optical microscopy (a) and electron microscopy (b) it is observed that the $VB_2$ particles have large dimensions, up to 24µm. Fig. 9 shows the peaks of the $VB_2$compound.

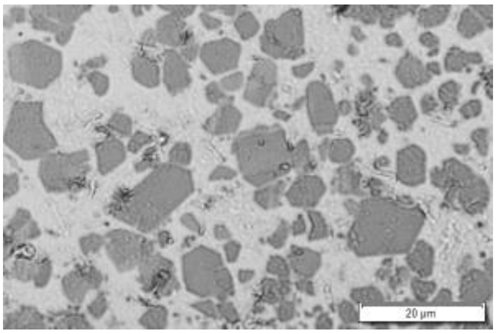


(a)

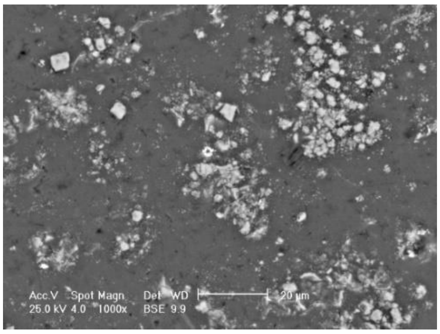


(b)

Fig. 8. Optical microstructure (a) and SEM micrograph of the AA6063/$VB_2$ composites

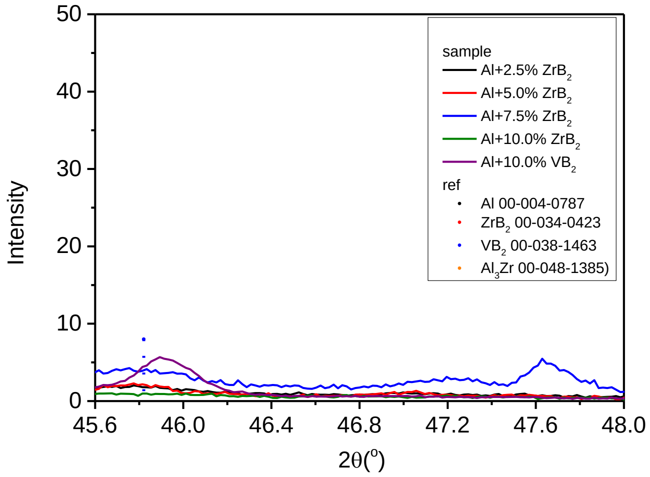


Fig. 9. X-ray diffraction of the AA6063/$ZrB_2$ and AA6063/$VB_2$ composites, with highlighted $VB_2$ peaks

The obtained $VB_2$ compound crystallizes in the hexagonal system, with structure type $AlB_2$, Pearson symbol hP3, space group P6/mmm with lattice parameters a = 0.2998 nm, c = 0.3056 nm and the calculated density $\rho$ = 5.066 $g/cm^3$.

## 4. Conclusions

Upon obtaining in-situ metal-matrix composites by the aluminothermic reaction between AA6060/AA6063 alloys, $K_2TiF_6$, $K_2ZrF_6$, $KBF_4$ salts and AlV10 pre-alloy, in the presence of cryolite ($Na_3AlF_6$), results in $TiB_2$, $TiAl_3$, $TiAl_2$, $ZrB_2$, $Al_3Zr$ and $VB_2$ intermetallic compounds, as can be seen from the diffractions presented in the figures 4, 6, 7 and 9. The concentration of these compounds is given by the quantities of salts used, relative to the matrix and the reaction time.

In the elaboration of the AA6060, AA6063 / $MeB_2$ composites the aim is to obtain borons with special properties (high hardness).

If the aluminothermic reactions are not completed, the resulting compounds crystallize in symmetry systems with lower atomic density (rhombic, tetragonal) and have lower properties.:

- $TiB_2$ – hexagonal system, 3370 HV hardness, density 4.52 g / $cm^3$ compared to $TiAl_3$ – tetragonal system, micro-hardness 2381 HV, density 4.0 g/$cm^3$ or $TiAl_2$ – rhombic system, 2029 HV micro-hardness, density 3.51 g/$cm^3$.
- $ZrB_2$ – hexagonal system, 3400 HV hardness, density 6.104 g/$cm^3$ compared to $ZrAl_3$ – tetragonal system, micro-hardness 2834 HV, density 4.117 g/$cm^3$.

In the case of the AA6063/$VB_2$ composite, no intermetallic compounds were obtained from crystallographic systems with low compactness, but only $VB_2$ - hexagonal system, hardness 4234 HV, density 5.066 g/$cm^3$.

Analysing the results, the crystalline structure of the $TiB_2$ compound obtained presents the same crystallographic system (hexagonal, P6/mmm) with small differences for the lattice parameters: a = 0.30325 nm compared to a = 0.3028 nm and c = 0.32313 nm compared to c = 0.3228 nm from reference [16]. There are other opinions about its structure [17, 18], considering that it crystallizes in the tetragonal system with the lattice parameters a = 0.611 nm, c = 0.456 nm.

For $TiAl_3$ the same crystallographic system (tetragonal, I4/mmm) was obtained, with small differences for the network parameters: a = 0.384 nm against a = 0.38537 nm and c = 0.859 nm against c = 0.8583 nm from the reference [16]. Hansen [17] and Barabas [18] consider that $TiAl_3$ has a tetragonal structure (type $D0_{22}$), with the lattice parameters a = 0.5435 nm, c = 0.8591 nm.

The obtained $TiAl_2$ particles presents the following characteristics: rhombic system, Cmmm space group with network parameters a = 0.120944 nm, b = 0.3959 nm, c = 0.40315 nm, with the calculated density $\rho$ = 3.51 g/$cm^3$, same as in reference [16]. For $Al_2Ti$, other specialists [17, 18] considers it to crystallize in the tetragonal system (with structure type $Ga_2Hf$), with the Pearson Symbol tI24, space group $I4_1$/amd, with the lattice parameters a = 0.3976 nm, c = 2.436 nm.

The obtained $ZrB_2$ particles have the following characteristics: hexagonal system, with type $AlB_2$ structure, Pearson symbol hP3, space group P6 / mmm with lattice parameters a = 0.3169 nm, c = 0.3530 nm, calculated density $\rho$ = 6.104 g/$cm^3$, compared to a = 0.3170(3)nm and compared to c = 0.3533nm from the references [14] [15] [17].

The obtained $Al_3Zr$ particles have the following characteristics: tetragonal system, with $Al_3Zr$ type structure, Pearson symbol tI16, I4/mmm space group with lattice parameters a = 0.4009 nm, c = 1.7281 nm, calculated density ρ = 4.117 g/cm$^3$ or a = 0.4015 nm and c = 1.7316 nm from [14] [15] [17].

The obtained $VB_2$ particles have the following characteristics: hexagonal system, with type $AlB_2$ structure, Pearson symbol hP3, space group P6 / mmm with lattice parameters a = 0.2998 nm, c = 0.3056 nm, calculated density ρ = 5.066 g/cm$^3$ or a = 0.2994 nm and c = 0.3048 nm from [14] [15] [17].

**Acknowledgements**

The work has been funded by the Operational Programme Human Capital of the Ministry of European Funds, Work-based learning systems through entrepreneur scholarships for doctoral and post-doctoral students through the Financial agreement 51668/09.07.2019, SMIS code 124705.

## R E F E R E N C E S

[1] V. S. Zolotorevsky, N. A. Belov și M. V. Glazoff, în *Casting Aluminium Alloys*, Elsevier Science, 2007, p. 544.

[2] J. T. Healey, Guinier-Preston zone evolution in 7075 aluminium, University of Florida, 1976.

[3] H. Feufel, T. Gödecke, H. Lukas și F. Sommer, „Investigation of the Al-Mg-Si System by Experiments and Thermodynamic Calculations," Alloys Compd., 1997, pp. 31-42.

[4] O. Barabash, O. Sulgenko, T. Legkaya și N. Korzhova, „Experimental Analysis and Thermodynamic Calculation of the Structural Regularities in the Fusion Diagram of the System of Alloys Al-Mg-Si," în *Calculation, Equi.Diagram, Experimental*, J. Phase Equilib., 2001, pp. 5-11.

[5] S.-P. Li, S.-X. Zhao, M.-X. Pan, D.-Q. Zhao, X.-C. Chen și O. Barabash, „Eutectic Reaction and Microstructural Characteristics of Al(Li)-Mg2Si Alloys," *J. Mater. Sci.*, vol. 36, nr. 10, pp. 1569-1575, 2001.

[6] S.-P. Li, S.-X. Zhao, M.-X. Pan, D.-Q. Zhao, X.-C. Chen și O. Barabash, „Design of New Cast Aluminium Materials Using Properties of Monovariant Eutectic Transformation Al+Mg2Si," *Mater. Sci. Forum,* Vol. %1 din %2396-403, nr. 9, pp. 729-734, 2002.

[7] T. Goedecke, „Direction of Crystallisations Paths in Ternary As-cast Alloys," *Z. Metallkd.,* vol. 2001, nr. 92, pp. 966-978, 2001.

[8] E. Schürmann și A. Fischer, „Equilibria with Liquid in the Aluminium- Magnesium-Silicon Ternary System, Part 3, Al-Mg-Si System," *Giessereiforschung,* vol. 29, nr. 14, pp. 161-165, 1977.

[9] O. Barabash, Y. Milman, N. Korzhova, T. Legkaya și Y. Podrezov, „esign of New Cast Aluminium Materials Using Properties of Monovariant Eutectic Transformation L-Al+Mg2Si," *Mater. Sci. Forum.,* Vol. %1 din %2396-402, nr. 9, pp. 729-734, 2002.

[10] K. H. Kumar, N. Chakraboti, H.-L. Lukas, O. Bodak și L. Rokhlin, „Al-Mg-Si (Aluminium - Magnesium - Silicon)," în *Light Metal Systems. Part 3,* Berlin, Springer-Verlag, 2005.

[11] H. Philips, „Annotated Equilibrium Phase Diagrams of Some Aluminum Alloy Systems,"

London, Monograph 25, 1959.

[12] L. Mondol'fo, în *Aluminum Alloys – Structure and Properties*, Boston, Butterworth, 1976, p. 424.

[13] I. Kolobnev, „Zharoprochnost'liteinyh alyuminievyh splavov," Moscow, Metallurgiya, 1973, p. 320.

[14] J. Daams, P. Villars și J. v. Vucht, Atlas of crystal structure for intermetallic phases, ASM International, 1991.

[15] ASM Handbook, „Metallography And Microstructures," ASM International, 1992, pp. 1566-1568.

[16] W. Warlimont și H. Martienssen, Springer Handbook of Condensed Matter and Materials Data, Berlin: Spinger Berlin Heidelberg New York, 2005.

[17] M. Hansen, Constitution of binary alloy, Metallurgical Engineering Series, New York: McGraw-Hill Book Company Inc, 1958.

[18] O. Barabaş şi I. N. Kovali, Structura cristalină a metalelor şi aliajelor, Kiev, 1986.